

# **Thin-film composite forward osmosis membranes based on polysulfone supports blended with nanostructured carbon materials**

Sergio Morales-Torres\*, Carla M.P. Esteves, José L. Figueiredo, Adrián M.T. Silva

*Laboratory of Separation and Reaction Engineering – Laboratory of Catalysis and Materials (LSRE-LCM), Faculdade de Engenharia, Universidade do Porto, Rua Dr. Roberto Frias, 4200-465 Porto, Portugal.*

\*Corresponding author: [semoto@fe.up.pt](mailto:semoto@fe.up.pt).

## **Abstract**

Polysulfone (PSf) membrane supports were blended with pristine multi-walled carbon nanotubes (MWCTNs), functionalized MWCNTs (MWf), graphene oxide (GO) and their corresponding carbon-TiO<sub>2</sub> composites. The surface hydrophilicity and the porous structure of the supports depended markedly on loading, type and surface chemistry of the nanostructured material, as well as on the addition or not of polyvinylpyrrolidone (PVP). These PSf supports were used to develop polyamide thin-film composite (TFC) membranes, whose performance was evaluated in forward osmosis using distilled water and 0.6 M NaCl solutions. TFC membranes prepared on PSf supports containing MWf and GO showed higher water permeation and draw solute rejection than those with hydrophobic MWCNTs or neat PSf only. An improved performance was observed when both carbon-TiO<sub>2</sub> composites and PVP were used, due to a porous structure of more elongated and straight finger-like pores and enhanced hydrophilicity. Among them, the most permeable membrane was that containing 0.5 wt.% of a GO-TiO<sub>2</sub> composite and PVP (12.5 L m<sup>-2</sup> h<sup>-1</sup> of water flux; ca. 60% higher than a TFC membrane on a commercial PSf support). However, the best performing membrane with the lowest specific solute flux (0.41 g L<sup>-1</sup>) was that obtained when replacing GO by MWf.

**Keywords:** *Forward osmosis; carbon nanotubes; graphene oxide; polysulfone; thin-film composite membranes.*

## 1. Introduction

Natural water supplies are becoming scarce and/or contaminated in some regions of the world, seawater desalination offering an excellent solution to mitigate the problem. Among the available desalination technologies, forward osmosis (FO) is receiving much attention [1]. In this process, a selective semipermeable membrane separates two solutions with different concentrations: a feed solution and a more concentrated draw solution. By using the osmotic pressure difference to transport the water molecules across the membrane, FO may overcome some limitations typically faced by reverse osmosis (RO) (such as membrane lifetime and energy consumption), mainly in desalination of high-salinity brines or industrial wastewaters [2, 3]. Even so, the implementation of FO in desalination still poses crucial challenges such as fouling, reverse solute diffusion and internal concentration polarization (ICP), and thus novel membranes and draw solutes are under development [4].

FO membranes available in the market mainly consist of cellulose triacetate membranes or thin-film composite (TFC) membranes composed by two layers: a porous membrane support and an active skin layer of polyamide. The reverse solute diffusion is mainly controlled by the chemical properties of the active layer, while high water fluxes and reduced ICP are achieved by minimizing the so-called structural parameter ( $S$ ) of the support. The  $S$  parameter proportionally increases with the thickness and tortuosity of the support, and decreases as the porosity increases [2]. The hydrophilicity of the support also plays an important role on the performance [5].

Polysulfone (PSf) membranes are widely used as supports for TFC membranes in water applications, but their hydrophobic character decreases the effective porosity of the membrane when immersed in water, and is also responsible for higher fouling and shorter lifetime. One approach to enhance the hydrophilicity of PSf membranes is by blending a surface modifier or filler of hydrophilic nature, such as silica ( $\text{SiO}_2$ ) [6, 7], titanium dioxide ( $\text{TiO}_2$ ) [8, 9], zeolites [10, 11], halloysite nanotubes ( $\text{Al}_2\text{Si}_2\text{O}_5(\text{OH})_4 \cdot 2\text{H}_2\text{O}$ ) [12] and, more recently, nanostructured

carbon materials [13-17]. Multi-walled carbon nanotubes (MWCNTs) and graphene derivatives such as graphene oxide (GO) and reduced GO (rGO), are interesting alternatives due to their transport characteristics, huge strength, smooth structure and easily tunable surface chemistry [18-21]. The incorporation of oxygen-containing surface groups in these materials increases their hydrophilicity and, as consequence, improves their dispersion in specific solvents and polymers [14, 22], which may affect the membrane properties.

In the particular case of TFC membranes, the incorporation of MWCTNs, GO and rGO has been accomplished following the strategy described above (i.e., by blending the nanostructured carbon material with the support matrix) or by adding the carbon material into the active layer (also known as thin-film nanocomposite –TFN– membranes). Wang *et al.* [23] used carboxylated MWCNTs (2 wt.% optimum loading) in polyethersulfone (PES) supports to fabricate TFC membranes with water fluxes higher than the unmodified PES support. In a subsequent study [17], rGO modified graphitic carbon nitride (0.5 wt.%) was used to enhance the membrane performance. Park *et al.* [24] reported that the addition of GO (0.25 wt.%) in TFC membranes favoured the formation of the active layer and enhanced water permeability. On the other hand, TFN membranes containing MWCNTs (0.1 wt.%) functionalized with amine groups exhibited 160% higher water flux than the control TFC membrane (without MWCNTs), although the salt rejection was not remarkable [25]. In a recent work, Song *et al.* proposed [26] the incorporation of pristine CNTs (0.05 wt.%) in both active and support layers, leading to a double-skinned TFN membrane with an excellent solute rejection and a water flux 54% higher than the double-skinned TFC membrane without CNTs. The effect of adding GO (400-600 ppm) in TFN membranes also allowed to enhance the water flux under reasonable draw solute rejections [27]. Regarding a particular application in RO, instead of FO, GO (0.12 wt.%) improved the water flux obtained with TFN membranes (up to 80%) without significantly affecting salt selectivity [28]. Yin *et al.* [29] proposed that GO nanosheets may serve as water channels when incorporated in TFN membranes, although a lower optimum GO loading (0.015 wt.%) was reported. The water flux of

TFN membranes containing carboxy-functionalized MWCNTs (0.1 wt.%) was improved almost twice without sacrificing solute rejection ( $> 90\%$ ), showing better antifouling and antioxidative properties than the control TFN membrane [30]. PSf membranes containing MWCNTs (0.1 wt.%) functionalized with polydopamine presented a high mechanical strength, enhanced permeability and good rejections (99.98%) using bovine serum albumin (BSA) solution, but membranes modified with polydopamine-MWCNTs presented lower water permeability than their analogues with acid-MWCNTs [31].

Therefore, in general, the incorporation of MWCNTs, GO and rGO into the support of TFC membranes resulted in an improved membrane performance by enhancing the surface hydrophilicity and by minimizing the structural parameter ( $S$ ), consequently lowering ICP. On the other hand, the direct addition of these carbon materials into the active layer allowed enhancing the surface hydrophilicity, and the fouling and chlorine resistances. According to the referred works, the optimum material loading for TFC membranes was between 0.015 and 0.5 wt.%, depending on the different functionalization treatments performed on MWCNTs or GO, the layer where the carbon material was incorporated (support or active layer), as well as the synthesis conditions used in the development of these membranes, among others. This broad interval of carbon material loadings hinders the adequate comparison between MWCNTs and GO when used to prepare TFC membranes.

In the present work, the incorporation of nanostructured carbon-based materials into the support of TFC membranes was investigated. In particular, PSf membrane supports blended with pristine MWCNTs, functionalized MWCNTs and GO were prepared to study the effect of loading, type and surface chemistry of these materials on the hydrophilicity and structure of the membranes. Furthermore, these chemical and structural properties were also investigated for PSf supports prepared with a pore forming agent (polyvinylpyrrolidone, PVP) and/or carbon-TiO<sub>2</sub> composites. Selected supports were then used to prepare TFC membranes and to assess their

performances in terms of water permeation and reverse solute diffusion in FO experiments. To the best of our knowledge, carbon-TiO<sub>2</sub> composites, in particular using functionalized MWCNTs or GO, were not previously incorporated into supports of TFC membranes for FO, although some works were reported for RO [32, 33] and nanofiltration [34].

## 2. Experimental

### 2.1. Materials

Polysulfone Udel<sup>®</sup> P-3500 LCD MB3 polymer, kindly supplied in pellet form by Solvay, was used to prepare the PSf supports. Polyvinylpyrrolidone (PVP, 10 kDa) and 1-methyl-2-pyrrolidinone (NMP, 99.5%) obtained from Sigma-Aldrich were used as pore forming agent and solvent, respectively, to develop PSf supports. *m*-Phenylenediamine (MPD, 99%) and 1,3,5-benzenetricarbonyl trichloride (TMC, 98%) from Sigma-Aldrich were used to prepare TFC membranes (i.e., using PSf as supports). Sodium chloride (NaCl, 99.5%) and *n*-hexane (C<sub>6</sub>H<sub>6</sub>, >99%) were supplied by Merck, while nitric acid (HNO<sub>3</sub>, 65 wt.%) was obtained from Fluka. Commercial PSf membranes (HT Tuffryn<sup>®</sup> with 0.2 μm pore size and 25 mm diameter) were purchased from Pall Corporation and used as reference membrane supports.

### 2.2. Synthesis of nanostructured carbon materials and carbon-TiO<sub>2</sub> composites

Pristine MWCNTs prepared by CVD were supplied by Nanocyl<sup>™</sup> (NC3100 series), while functionalized MWCNTs were obtained by a HNO<sub>3</sub> hydrothermal oxidation method [22]. The pristine and functionalized MWCNTs will be referred hereafter as MWp and MWf, respectively. On the other hand, an aqueous suspension of GO was obtained by sonicating graphite oxide prepared following a modified Hummers method [35].

Carbon-TiO<sub>2</sub> composites were synthesized by liquid phase deposition method according to our previous works [36, 37]. The carbon-TiO<sub>2</sub> composites will be denoted as GOT or MWfT, which refers to the type of carbon material used, GO or MWf, respectively. Commercial TiO<sub>2</sub>

(Degussa P25 from Evonik) without the addition of carbon material was used as reference (hereafter referred as P25). The detailed procedure for preparation of the materials is given in Section S1, Supporting Information.

### *2.3. Preparation of PSf supports and TFC membranes*

PSf supports blended with nanostructured materials were prepared by a non-solvent induced phase separation method studying different synthesis parameters such as addition of PVP and loading, type and surface chemistry of nanostructured carbon materials (i.e., MWp, MWf or GO), as well as their corresponding carbon-TiO<sub>2</sub> composites (i.e., MWfT or GOT), including P25 as reference. In some cases, PVP (5 wt.%) was added as pore forming agent. Neat PSf supports were also prepared following the same experimental procedure but without any amount of nanostructured material added. Both bench-prepared PSf and commercial PSf supports were used to prepare TFC membranes following a methodology adapted from [9]. The detailed procedure for fabrication of the PSf supports and TFC membranes is provided in Sections S2 and S3, Supporting Information, respectively.

The PSf supports were labelled as follows: XY/S-P, where X is the amount of nanostructured material used (ranging from 0.05 to 0.5 wt.%); Y indicates the type of material used, i.e. MWp (pristine MWCNTs), MWf (functionalized MWCNTs), GO (graphene oxide), MWfT (MWf-TiO<sub>2</sub> composite), GOT (GO-TiO<sub>2</sub> composite) or P25 (bare TiO<sub>2</sub>); P indicates the presence of PVP. The nomenclature and composition of the prepared PSf supports are summarized in Table 1. TFC membranes are referred by using “M” instead of “S” to the corresponding support label, i.e., XY/M-P instead of XY/S-P (e.g., 0.1MWp/M-P would be the TFC membrane prepared on the 0.1MWp/S-P support).

**Table 1.** Labels and chemical compositions of the PSf supports.

Support label	Nanostructured material		PVP (wt.%)
	(type)	(wt.%)	
S	-	-	-
S-P	-	-	5
0.05MWp/S	MWp	0.05	-
0.1MWp/S	MWp	0.1	-
0.3MWp/S	MWp	0.3	-
0.5MWp/S	MWp	0.5	-
0.1MWf/S	MWf	0.1	-
0.1GO/S	GO	0.1	-
0.05MWp/S-P	MWp	0.05	5
0.1MWp/S-P	MWp	0.1	5
0.3MWp/S-P	MWp	0.3	5
0.5MWp/S-P	MWp	0.5	5
0.1MWf/S-P	MWf	0.1	5
0.1GO/S-P	GO	0.1	5
0.5MWfT/S-P	MWfT	0.5	5
0.5GOT/S-P	GOT	0.5	5
0.5P25/S-P	P25	0.5	5

#### 2.4. Characterization of nanostructured materials, PSf supports and TFC membranes

The morphological analysis of the samples was studied by scanning electron microscopy (SEM) using a FEI Quanta 400FEG ESEM/EDAX Genesis X4M instrument. The mean pore diameter ( $d_{\text{pore}}$ ) was determined for each membrane using Image J software. The specific surface area ( $S_{\text{BET}}$ ) [38] and the total pore volume ( $V_{\text{pore}}$ ) [37, 39] were calculated from N<sub>2</sub> adsorption-desorption isotherms at -196 °C using a Quantachrome NOVA 4200e, while the overall porosity ( $\epsilon$ ) of the membranes was determined by the gravimetric method [21]. The hydrophilicity/hydrophobicity of the membrane surface was determined by water contact angle measurements using an Attension optical tensiometer (model Theta) [40]. The surface chemistry of the carbon materials was characterized by temperature programmed desorption (TPD) and pH measurements of point of zero charge ( $\text{pH}_{\text{PZC}}$ ) [37, 41]. Viscosity of selected dope solutions was measured at 25 °C using a controlled stress rheometer (ARG2, TA Instruments). More information about the methods used is included in Section S4, Supporting Information.

## 2.5. Evaluation of FO performance

The performance of bench-prepared TFC membranes was evaluated in a home-made FO unit (Figure S1). In a typical run, the membrane was placed into a “H-shaped” glass module operating in co-current flow (effective membrane area of 2 cm<sup>2</sup>) at room temperature. Then, DI water (feed) and a 0.6 M NaCl solution (draw) were pumped in recirculation mode at a linear velocity of 0.09 cm s<sup>-1</sup> for 150 min. Each TFC membrane was evaluated under the pressure retarded osmosis (PRO) mode (i.e., active layer facing the draw solution) and FO mode (i.e., active layer facing the feed solution).

The most efficient TFC membrane (0.5MWfT/M-P) was also tested by using: (i) different NaCl (draw) concentrations, i.e., 0.6, 1.0 and 2.0 M; (ii) different types of draw solutions: KCl, MgCl<sub>2</sub> and MgSO<sub>4</sub>; and (iii) a different membrane module configuration (W-cell).

The water flux ( $J_w$ ) was calculated by measuring the weight changes of the feed solution by applying Eq. 1

$$J_w = \frac{\Delta V}{A_m \times \Delta t} \quad (1)$$

where  $J_w$  is the permeate flux (L m<sup>-2</sup> h<sup>-1</sup>, LMH),  $\Delta V$  is the permeate volume (L),  $A_m$  is the effective area of the membrane (m<sup>2</sup>), and  $\Delta t$  is the sampling time (h).

Ionic conductivity was measured in both feed and draw streams by using online conductivity meters (VWR mod. 310) and ion chromatography (Metrohm, mod. 881 Compact IC pro) to determine the reverse solute flux by applying Eq. 2:

$$J_s = \frac{\Delta(C_t \times V_t)}{A_m \times \Delta t} \quad (2)$$

where  $J_s$  is the solute reverse flux (g m<sup>-2</sup> h<sup>-1</sup>, gMH),  $C_t$  is the solute concentration (determined by ion chromatography) and  $V_t$  is the volume in the feed solution at a given time (h).

### 3. Results and discussion

#### 3.1. Characterization of the nanostructured carbon materials and the carbon-TiO<sub>2</sub> composites

The morphology of the nanostructured materials before their incorporation in PSf supports was studied by SEM. Representative SEM micrographs of MWp, MWf, GO, MWfT, GOT and P25 are shown in Figures 1a-f, respectively. Both MWp (Figure 1a) and MWf (Figure 1b) consist of agglomerated CNTs, while GO (Figure 1c) presents a layered structure. For the composites, the morphology depends on the nanostructured carbon material used and the accessibility for TiO<sub>2</sub> assembling during the preparation method. Clusters of TiO<sub>2</sub> particles surrounded by CNTs were observed for MWfT (Figure 1d - inset), while a homogeneous assembly of TiO<sub>2</sub> particles on both sides of GO layers was observed for GOT (Figure 1e). In the case of P25 (Figure 1f), the typical structure of TiO<sub>2</sub> particles was revealed.

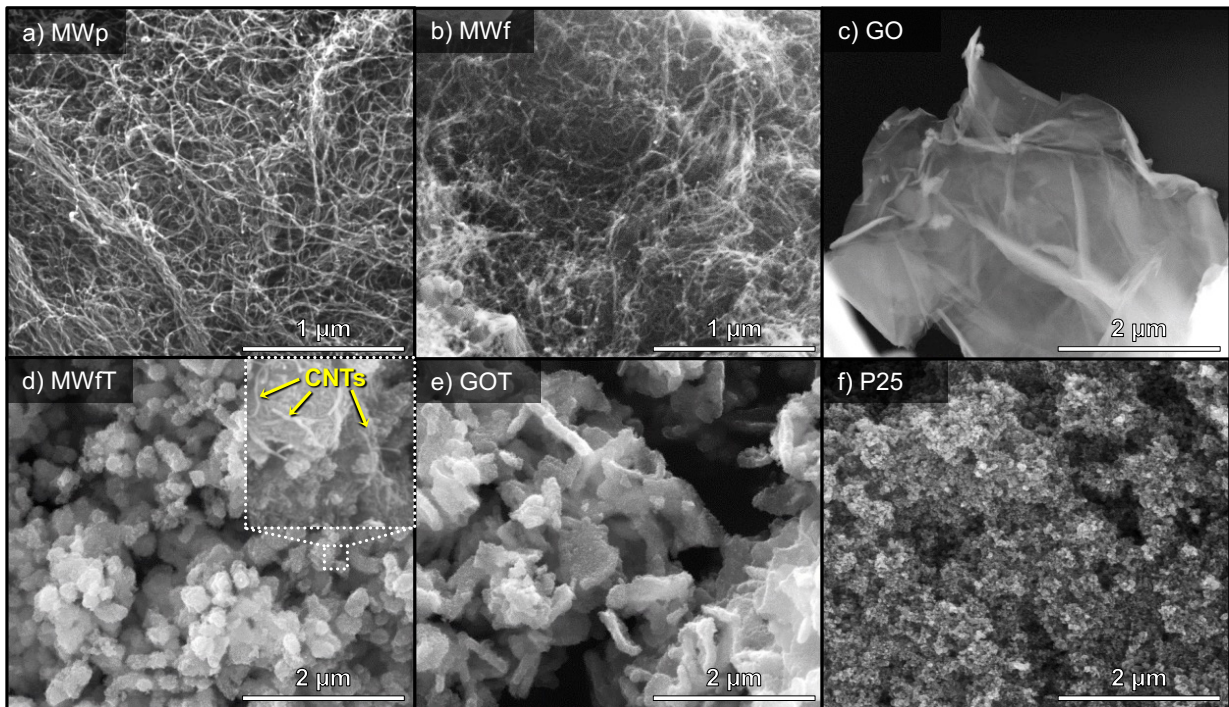


**Figure 1.** SEM micrographs for the nanostructured carbon materials (a-c), the corresponding carbon-TiO<sub>2</sub> composites (d, e) and the P25 material (f).

The different morphologies of the materials obviously have influence on their textural characteristics (Table 2). Thus, the BET specific surface area ( $S_{\text{BET}}$ ) and the total pore volume

( $V_{\text{pore}}$ ) were determined, GO presenting the lowest  $S_{\text{BET}}$  ( $21 \text{ m}^2 \text{ g}^{-1}$ ) and  $V_{\text{pore}}$  ( $0.03 \text{ cm}^3 \text{ g}^{-1}$ ) due to the stretched assembly of the GO sheets, originated by strong hydrogen bonding when the suspension was dried to perform the  $\text{N}_2$  adsorption analysis [36]. Both MWp and MWf materials presented the largest porosity due to their significant exposed structure formed by CNT bundles, and the higher  $S_{\text{BET}}$  determined for MWf can be due to the removal of amorphous carbon present on the bundles during the  $\text{HNO}_3$  hydrothermal oxidation [22]. Regarding the carbon- $\text{TiO}_2$  composites, both MWfT and GOT presented higher  $S_{\text{BET}}$  and  $V_{\text{pore}}$  than P25, although different trends were observed depending on the type of material used. In fact, MWfT has a lower  $S_{\text{BET}}$  than GOT, probably due to the better distribution of  $\text{TiO}_2$  particles on GO sheets rather than in CNTs (Figure 1e vs. d, respectively), a significant development of the porosity (i.e.,  $S_{\text{BET}}$  and  $V_{\text{pore}}$ ) being observed for GOT in comparison with GO.

**Table 2.** Textural and chemical properties of the nanostructured carbon materials and the corresponding carbon- $\text{TiO}_2$  composites.

Sample	$S_{\text{BET}} (\pm 5 \text{ m}^2 \text{ g}^{-1})$	$V_{\text{pore}} (\pm 0.01 \text{ cm}^3 \text{ g}^{-1})$	$\text{O}_{\text{TPD}} (\pm 0.1 \text{ wt.}\%)$	$\text{pH}_{\text{PZC}} (\pm 0.1)$
MWp	315	0.77	0.4	7.0
MWf	400	0.65	9.2	4.4
GO	21	0.03	23.6	2.8
MWfT	86	0.16	-	3.6
GOT	117	0.17	-	3.2
P25	55	0.13	-	6.3

The surface chemistry of the carbon materials was modified by introducing oxygen-containing functional groups originating hydrophilic materials (MWf and GO). The oxygen content ( $\text{O}_{\text{TPD}}$ , Table 2) determined from the amounts of CO and  $\text{CO}_2$  evolved during TPD experiments was higher for GO than for MWf (23.6 wt.% and 9.2 wt.%, respectively). The  $\text{HNO}_3$  hydrothermal oxidation performed over MWp was less severe than the method used for the synthesis of GO, the later including stronger oxidants such as  $\text{H}_2\text{SO}_4$  and  $\text{KMnO}_4$ . Furthermore,

the graphitic structure of the carbon material and the surface accessibility to be oxidized could also contribute to the larger functionalization obtained for GO. In general, the presence of oxygen-containing groups improves the interaction between the carbon phase and the TiO<sub>2</sub> particles by means of Ti–O–C bonds [42]. The low pHPZC values for MWfT, GO and GOT (Table 2) indicate a higher acidity in comparison to the other materials. The surface chemistry of GO should be responsible not only for its high dispersion in the solution during the preparation of the composites, but also for the good assembly of the TiO<sub>2</sub> particles on GO [43], as observed by SEM (Figure 1e).

### 3.2. Characterization of the membranes

#### 3.2.1. Structure of PSf and PSf-PVP supports blended with nanostructured carbon materials

The morphology of the neat PSf support (referred to “S”) and PSf supports blended with nanostructured materials (XY/S) and also with PVP (XY/S-P) was studied by SEM. Figures 2 and 4 show representative SEM images of the top surfaces and cross-sections (at the same magnifications), respectively. All PSf supports presented a comparable dense top surface with no open pores (Figures 2a, b, d and e), although a structure of interconnected sponge-like pores was revealed below the dense layer, when the sample was broken for SEM analysis (Figure 2c). The colour of the membrane surface varied from bright grey to dark grey when high material loadings were added. However, the incorporation of different types of materials (i.e., MWp, MWf and GO) and the addition of PVP, does not seem to affect significantly the surface topology of the modified supports (Figures 2b, d and e with their corresponding inset images), since the major differences were found at the bottom of the supports, as discussed below in terms of SEM analysis of their cross-sections. On the other hand, the surface of TFC membranes (i.e., XY/M and XY/M-P) was different from that of the respective supports (Figure 2f vs. b). TFC membranes showed a typical ridge-valley surface, resulting from the interfacial polymerization of MPD and TMC on the corresponding PSf support [9].

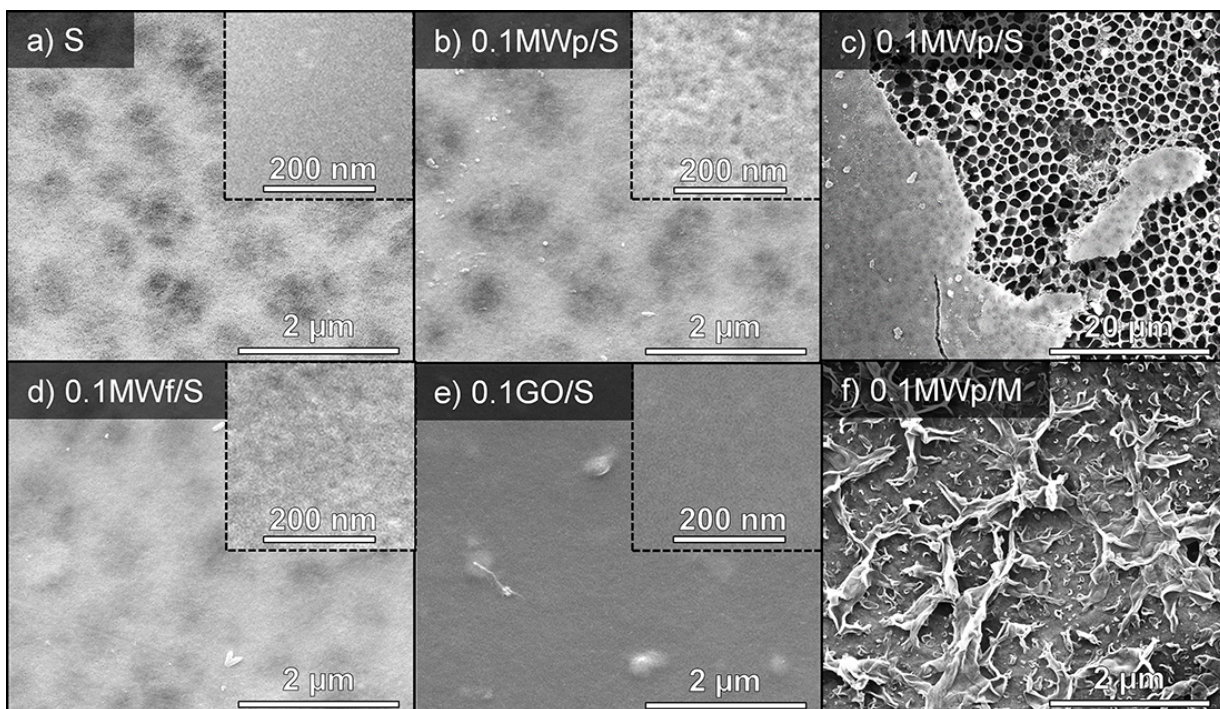


**Figure 2.** SEM micrographs of the top surface for neat PSf (a) and nanostructured material/PSf blended supports (b-e) (inset images show a higher magnification). The top surface for a TFC membrane is also shown as reference (f).

Regarding the cross-section micrographs (Figure 3), the supports consist of a typical asymmetric structure with a thin dense top-layer and a porous sub-layer. The morphology of the neat S support (Figure 3a) was different from that observed for PSf supports (without PVP) modified with nanostructured materials (Figures 3b-d); the support blended with hydrophobic MWp mainly presented macrovoids (Figures 3b and c), while those containing hydrophilic materials (MWf and GO) showed finger-like macrovoids (e.g., Figure 3d for 0.1MWf/S). Increasing MWp loadings above 0.3 wt.% led to the appearance of pinholes and CNT aggregates, which negatively influenced the mechanical stability and structure of the corresponding supports. The surface chemistry of the nanostructured carbon materials obviously affected the thermodynamic compatibility between the polymer and the solvent, in such manner that the addition of hydrophilic materials such as MWf and GO resulted in a faster onset of phase inversion, favouring the formation of larger finger-like macrovoids in the membranes [14, 24]. On the contrary, the addition of hydrophobic MWp led to a slower solvent/non-solvent exchange

during phase inversion, favouring the formation of sponge-like structures and large macrovoids. This phenomenon was more notorious when the viscosity of the membrane casting solution was enhanced by adding high MWp loadings (above 0.3 wt.%). In fact, the viscosity of the casting solutions varied from 41.85 to 244.2 Pa s when the MWp loadings used were 0.1 or 0.3 wt.%, respectively. Thus, the demixing process between solvent and non-solvent might have been retarded, the phase separation rate decreasing [15].

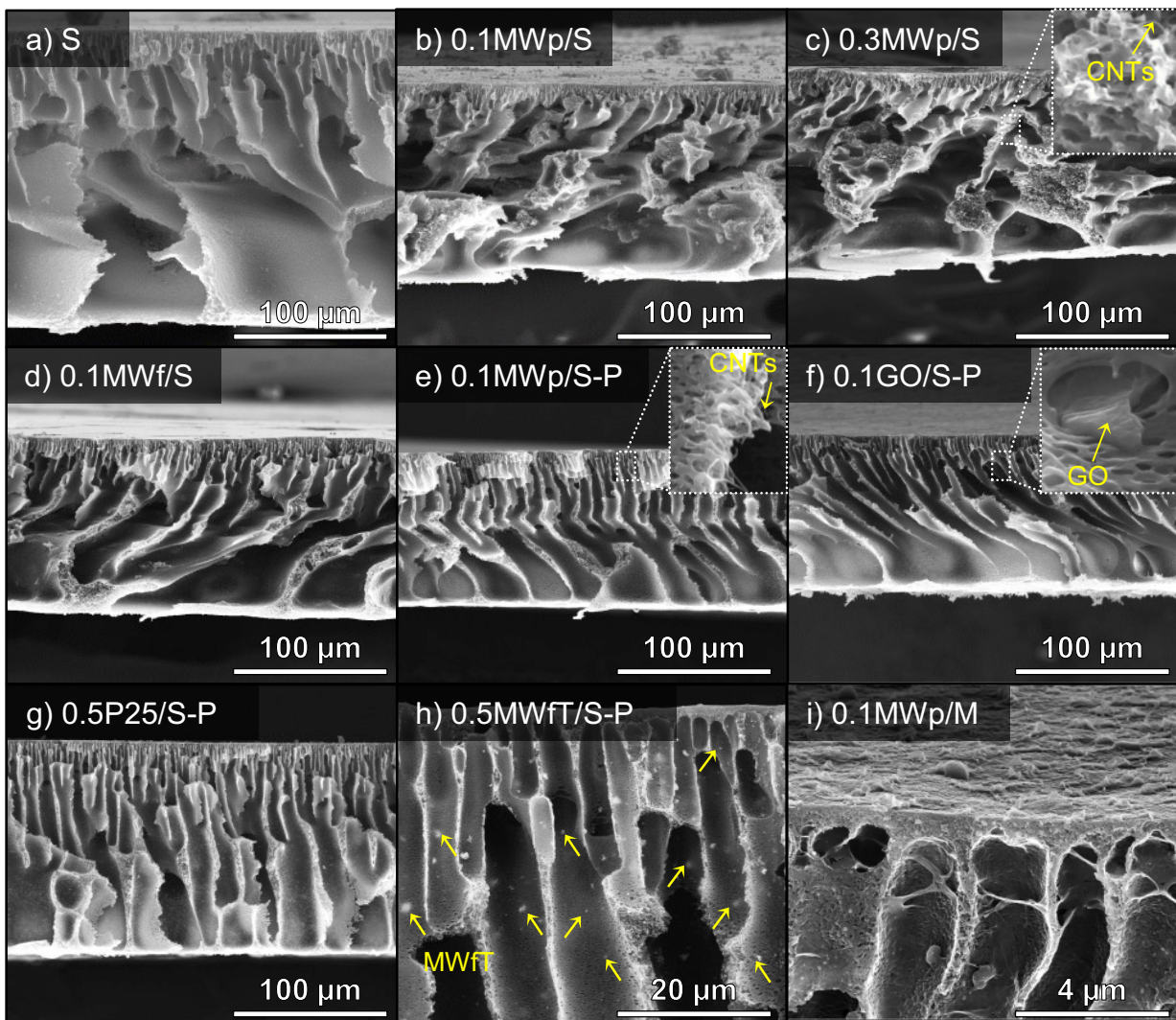


**Figure 3.** SEM micrographs of the cross-section for neat PSf (a) and nanostructured material/PSf blended supports (b-h) (inset images with higher magnification). The cross-section for a TFC membrane is also shown (i).

The formation of larger and elongated finger-like pores across the membrane was always favoured by the addition of PVP, regardless of the type and amount of material blended

(Figures 3e-h). In general, the nanostructured material was homogeneously dispersed throughout the support structure even at high loadings (Figure 3h for 0.5MWfT/S-P), although some isolated CNT bundles and GO sheets were also found through the finger-like pores of the supports (Figures 3e and f – insets, respectively). Furthermore, more elongated and straight finger-like pores were formed in supports blended with PVP and P25 or carbon-TiO<sub>2</sub> composites (Figures 3g and h, respectively). In these particular cases, the addition of TiO<sub>2</sub> nanoparticles allowed to increase the material loading up to 0.5 wt.%, which was also the optimum bare-TiO<sub>2</sub> loading reported by Emadzadeh *et al.* for modified PSf supports [44]. Therefore, the addition of PVP enhanced the hydrophilicity of the casting solution and decreased its viscosity (e.g., 1.792 and 8.862 Pa s for casting solutions containing 0.1 and 0.3 wt.% MWp, respectively, and PVP), the solvent/non-solvent exchange being accelerated and thus, favouring the formation of finger-like pores. This quicker solvent/non-solvent exchange was further evident when PVP and large loadings of carbon-TiO<sub>2</sub> composites or P25 were added in the membranes, since these materials presented larger amounts of hydroxyl groups in their structure [32-34, 44]. As an example, Figure 3i shows that the polyamide layer of TFC membranes was deposited onto the support surface and also into the network consisting of finger-like pores. During the interfacial polymerization, the monomers MPD and TMC react to form a highly cross-linked polyamide layer, which is confined to the region near the interface of two solutions containing the monomers [45]. Because the membrane support is soaked in the aqueous MPD solution before being contacted with the TMC solution, PSf supports with high porosity, high surface hydrophilicity and a smooth surface improve the contact between both monomers and, as consequence, the formation of the polyamide layer. This fact was recently described by Park *et al.* [24] for TFC membranes prepared on PSf supports containing well-dispersed GO.

The effect of different loading and type of material on the overall porosity of modified PSf and PSf-PVP supports was evaluated by applying the gravimetric method. Modified PSf supports presented always higher (or similar) values of porosity (78-85%) than those obtained for the neat

S support (78%) and the commercial Tuffryn PSf support (71%), regardless of the material type and loading (Figures 4a and b). In general, the overall porosity seems to increase with the use of hydrophilic materials (i.e., MWf and GO). However, this trend is less significant with PSf-PVP supports, probably because the addition of a pore forming agent, on its own, enhanced the porosity of the resulting supports (e.g., 85 and 89%, for 0.1GO/S and 0.1GO/S-P, respectively), even at high loadings of materials (e.g., 89% for 0.5GOT/S-P). PSf and PSf-PVP supports blended with a MWp loading above 0.3 wt.% presented lower porosity than the neat corresponding supports (Figure 4a). This less porous structure could be explained by the increased viscosity of the dope solution, which favours a slow solvent/non-solvent exchange during the phase inversion. Nevertheless, PSf-PVP supports blended with high loadings of hydrophilic material, i.e., 0.5 wt.% of GOT, MWfT or P25, presented an enhancement of the overall porosity, because the addition of TiO<sub>2</sub> nanoparticles improved the hydrophilicity of the membrane casting solution and thus, offset the effect of increased viscosity.

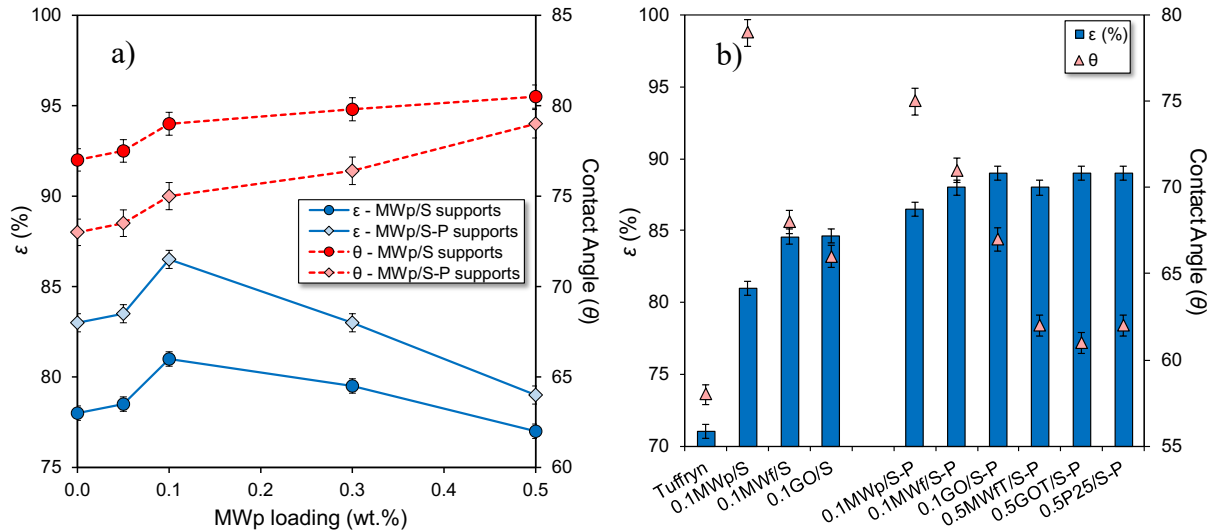


**Figure 4.** Dependency of the overall porosity ( $\epsilon$ ) and the contact angle ( $\theta$ ) for PSf and PSf-PVP supports blended with increasing MWp loadings (a) and different nanostructured materials (b). The data obtained for neat and commercial PSf supports are also included as reference.

The mean pore diameter ( $d_{\text{pore}}$ ) of the supports also seems to be influenced by the different loading, type and surface chemistry of the material, as well as by the addition of PVP. In general,

PSf supports blended with nanostructured materials presented larger pores ( $d_{\text{pore}} = 0.6\text{-}0.8 \mu\text{m}$ ) than those obtained with the neat S support ( $0.4 \mu\text{m}$ ) and commercial Tuffryn ( $0.2 \mu\text{m}$ ). Moreover, high MWp loadings seem to decrease the  $d_{\text{pore}}$  of the support, while pores slightly larger are obtained with the addition of hydrophilic materials (e.g.,  $d_{\text{pore}} = 0.7$  and  $0.8 \mu\text{m}$  for 0.1MWp/S and 0.1MWf/S, respectively). Supports containing PVP showed larger finger-like pores regardless of the type, load or chemical properties of the material blended, although slightly lower pore sizes were obtained for supports with high contents of hydrophilic materials (e.g.,  $d_{\text{pore}} = 2.4 \mu\text{m}$  for 0.5MWfT/S-P).

### 3.2.2. Surface hydrophilicity of PSf and PSf-PVP supports blended with nanostructured carbon materials

The surface hydrophilicity of modified PSf supports was markedly influenced by the surface chemistry of the material blended and the presence of PVP. Thus, hydrophilic materials such as MWf, GO, P25 and carbon-TiO<sub>2</sub> composites led to supports with lower contact angles than that obtained for the neat S support (e.g., 77°, 68° and 66° for S, 0.1MWf/S and 0.1GO/S, respectively) (Figure 4b). An increase of the hydrophobic MWp loading seems to produce PSf supports with higher contact angles (e.g., 77°, 79° and 81° for S, 0.1MWp/S and 0.5MWp/S, respectively) (Figure 4a). Supports prepared with PVP generally showed lower contact angles than those prepared without PVP (e.g., 80° and 76° for 0.3MWp/S and 0.3MWp/S-P, respectively) (Figure 4a). It is noteworthy to mention that the PSf supports with the lowest contact angles (around 61°) were those prepared with PVP and GOT, MWfT or P25, these values being comparable to that determined for the commercial Tuffryn membrane (58°) (Figure 4b).

### 3.3. Comparative performance of TFC membranes in forward osmosis

TFC membranes (i.e., M membranes) prepared by using PSf and PSf-PVP supports containing different loadings and types of nanostructured materials were tested in both PRO (active layer facing the draw solution) and FO modes (active layer facing the feed solution)

employing DI water and 0.6 M NaCl solution, as feed and draw solutions, respectively. TFC membranes were evaluated in terms of water flux ( $J_w$ ), reverse solute flux ( $J_s$ ) and specific solute flux ( $J_s/J_w$ ), as shown in Figures 5 and 6 for supports prepared without or with PVP, respectively.

The orientation of the active layer had a marked effect on the water flux of all membranes tested in this study; the membrane performance in PRO mode was always better than in FO (Figures 5 and 6), which might be attributed to the dilutive ICP effect when the active layer faces the feed solution [46]. As DI water was used as feed, water should flow with low resistance across the hydrophilic and porous substrate due to a very small concentrative ICP effect [47].

Regarding the PVP-free PSf supports (Figure 5a) tested in PRO mode, M membranes containing only hydrophilic materials (i.e., GO and MWf) presented higher water flux than the TFC membrane prepared on the neat S support (i.e., M), which could be due to the presence of finger-like macrovoids, a higher porosity (85% for both 0.1MWf/S and 0.1GO/S), a larger  $d_{\text{pore}}$  (0.8  $\mu\text{m}$ ) and a lower contact angle (68° and 66° for 0.1MWf/S and 0.1GO/S, respectively) of both supports compared to the neat S support (78%, 0.5  $\mu\text{m}$  and 78°). The addition of any hydrophobic MWp loading (i.e., 0.1MWp/S and 0.3MWp/S) did not improve the water flux in both operation modes, probably due the support structure formed by macrovoids, low porosity and surface hydrophilicity (e.g.,  $\varepsilon = 80\%$  and  $\theta = 81^\circ$  for 0.3MWp/S), which could adversely contribute to the ICP effect and the correct formation of the active layer during the development of TFC membranes [24]. This fact was more evident when membranes containing higher MWp loadings were compared, i.e.,  $J_w = 2.7$  and  $2.4 \text{ L m}^{-2} \text{ h}^{-1}$  in PRO mode for 0.1MWp/M and 0.3MWp/M, respectively.

The performance of these TFC membranes was also evaluated in terms of reverse solute flux (Figure 5b). TFC membranes tested in PRO mode presented always higher reverse solute fluxes than in FO due to the concentrations of solute at the membrane interfaces, which are related to both  $J_w$  and  $J_s$  in an analogous way [48]. In addition, the active layer of the TFC

membrane should hinder the draw solute reverse leakage through the membrane in FO mode [47]. Therefore, the reverse solute flux should increase *a priori* proportionally as the water flux. Nonetheless, M membranes containing hydrophilic carbon materials (i.e., MWf and GO) presented low salt leakage, even if they had high  $J_w$  values. On the contrary, 0.3MWp/M presented the highest salt leakage and the lowest  $J_w$  (Figures 5b and a). To clearly discriminate which is the best membrane in terms of clean water yield (i.e., without draw solute), the specific solute flux ( $J_s/J_w$  ratio) was calculated for M membranes (Figure 5c). In this context, 0.1MWf/M and 0.1GO/M were more efficient than the neat M membrane (e.g.,  $J_s/J_w = 0.74$ ,  $0.46$  and  $1.86$  g L<sup>-1</sup> in FO, respectively), while 0.3MWp/M was the worst ( $J_s/J_w = 3.93$  g L<sup>-1</sup>). Therefore, the chemical functionalization of the carbon materials seems to have a beneficial influence on the salt rejection of TFC membranes. The enhanced surface hydrophilicity of PSf supports by blending MWf or GO might have positively influenced the formation of the active layer during the development of TFC membranes [24], in contrast to 0.3MWp/M, presenting a high contact angle (80°). The improvement of salt rejection with oxidized CNT-based membranes was already reported by our group for direct contact membrane distillation of salty water, a correlation of the permeate flux with the amount of oxygen-containing groups created on CNTs being established [22]. Therefore, considering the results shown in Figure 5, the PSf support blended with 0.1 wt.% GO seems to be the best option to prepare TFC membranes for both PRO and FO modes.

In what concerns PSf-PVP supports, M-P membranes containing PVP and nanostructured materials (Figure 6) presented always a superior performance than their homologues without PVP (Figure 5). Considering a 0.1 wt.% material loading, M-P membranes containing the hydrophobic MWp showed higher water fluxes than those with hydrophilic carbon materials (MWf and GO), the flux values varying as follows:  $0.1MWp/M-P > 0.1GO/M-P > 0.1MWf/M-P$ . Since the porosity of these supports was comparable (ranging from 87% to 89%) and 0.1MWp/S-P had a higher contact angle, these results might be explained by an increase in the width of the elongated finger-like pores formed during the preparation of the PSf-PVP support, i.e.,  $d_{\text{pore}} = 3.0$  μm

(0.1MWp/S-P) > 2.5  $\mu\text{m}$  (0.1GO/S-P) > 2.0  $\mu\text{m}$  (0.1MWf/S-P). Therefore, the surface hydrophilicity induced by the addition of functionalized carbon materials seems to be less relevant for the water flux than the size of the finger-like pores. Thus, the largest  $d_{\text{pore}}$  of 0.1MWp/M-P allowed to achieve high water fluxes (11.5 and 10.8 L m<sup>-2</sup> h<sup>-1</sup> in PRO and FO modes, respectively), although it also favoured a high salt leakage (Figure 6b). Analogously to M membranes, M-P membranes with MWf or GO showed a higher selectivity towards NaCl, i.e., lower  $J_s/J_w$ , than that containing MWp (Figure 6c). Therefore, the addition of PVP to PSf supports might not influence the rejection properties of TFC membranes, this property being mainly affected by the addition of functionalized carbon materials. Once again, the M-P membrane with 0.1 wt.% GO was the most efficient, followed by that with 0.1 wt.% MWf and by 0.1 wt.% MWp.

Analogously to M membranes, a higher MWp loading did not enhance the water flux, nor the reverse solute flux of M-P membranes. As previously described, the addition of TiO<sub>2</sub> nanoparticles as P25 or carbon-TiO<sub>2</sub> composites enhanced the structure and hydrophilicity of the resulting PSf supports, the material loading being increased up to 0.5 wt.%, which was established as the optimum loading for TFC membranes [9, 44]. TiO<sub>2</sub> assembly onto the surface of carbon materials is intended to play a dual beneficial role: (i) to enhance the performance of modified TFC membranes due to a reduced ICP effect [8] and, (ii) to improve the dispersion of particles throughout the polymer matrix by reducing their agglomeration [32]. In this context, PSf-PVP supports blended with 0.5 wt.% of carbon-TiO<sub>2</sub> composites (i.e., GOT and MWfT) were used to prepare TFC membranes, and the results were compared with those containing P25 (as reference TiO<sub>2</sub> material). Figure 6a shows that all M-P membranes containing TiO<sub>2</sub> nanoparticles (i.e., P25, GOT and MWfT) showed higher water fluxes than their analogues prepared with hydrophilic carbon materials (GO and MWf). The addition of TiO<sub>2</sub> favoured a high surface hydrophilicity and a low tortuosity by the formation of more elongated and straight finger-like pores connecting both top and bottom layers of the support and, consequently, reducing its

structural parameter [8, 9]. The water fluxes obtained in PRO mode for these membranes varied as follows: 0.5P25/M-P ( $10.5 \text{ L m}^{-2} \text{ h}^{-1}$ ) < 0.5MWfT/M-P ( $11.5 \text{ L m}^{-2} \text{ h}^{-1}$ ) < 0.5GOT/M-P ( $12.5 \text{ L m}^{-2} \text{ h}^{-1}$ ). Because the surface hydrophilicity of these membranes was comparable, this trend might be explained by the differences found in their structural parameter and  $d_{\text{pore}}$ ; the 0.5GOT/S-P support presented the lowest  $S$  and the highest  $d_{\text{pore}}$ . The enhancement of water permeation with the  $d_{\text{pore}}$  for M-P membranes was previously pointed out for the case of 0.1MWp/M-P. On the other hand, the addition of carbon-TiO<sub>2</sub> composites to PSf-PVP supports not only increased the water fluxes, but also decreased the reverse solute fluxes obtained with the corresponding M-P membranes (Figure 6b). In particular, M-P membranes containing carbon-TiO<sub>2</sub> composites presented lower  $J_s$  values than that with P25 in both PRO and FO modes. Furthermore, the specific solute fluxes of both 0.5MWfT/M-P and 0.5GOT/M-P membranes were also lower than the M-P membrane containing only TiO<sub>2</sub> nanoparticles (0.5P25/M-P) (Figure 6c). Therefore, the use of carbon-TiO<sub>2</sub> composites into TFC membranes allowed to enhance the surface hydrophilicity, to reduce the structural parameter and to increase the selectivity towards NaCl.

Additionally, the performance of M-P membranes was compared with a TFC membrane prepared on the commercial PSf support (Tuffryn/M), better efficiencies being always obtained with all M-P membranes prepared in this study. It is noteworthy to indicate that Tuffryn/M had the worst solute rejection ( $J_s$ ).

Overall, the 0.5MWfT/M-P membrane presented the lowest  $J_s/J_w = 0.41 \text{ g L}^{-1}$  among the TFC membranes with a  $J_w \approx 8.4 \text{ L m}^{-2} \text{ h}^{-1}$  and a  $J_s \approx$  of only  $3.5 \text{ g m}^{-2} \text{ h}^{-1}$  in FO mode (Figure 6), while 0.1GO/M was the best performing membrane without PVP, resulting in  $J_s/J_w = 0.46 \text{ g L}^{-1}$ ,  $J_w \approx 3.6 \text{ L m}^{-2} \text{ h}^{-1}$  and  $J_s \approx 1.7 \text{ g m}^{-2} \text{ h}^{-1}$  in FO mode (Figure 5).

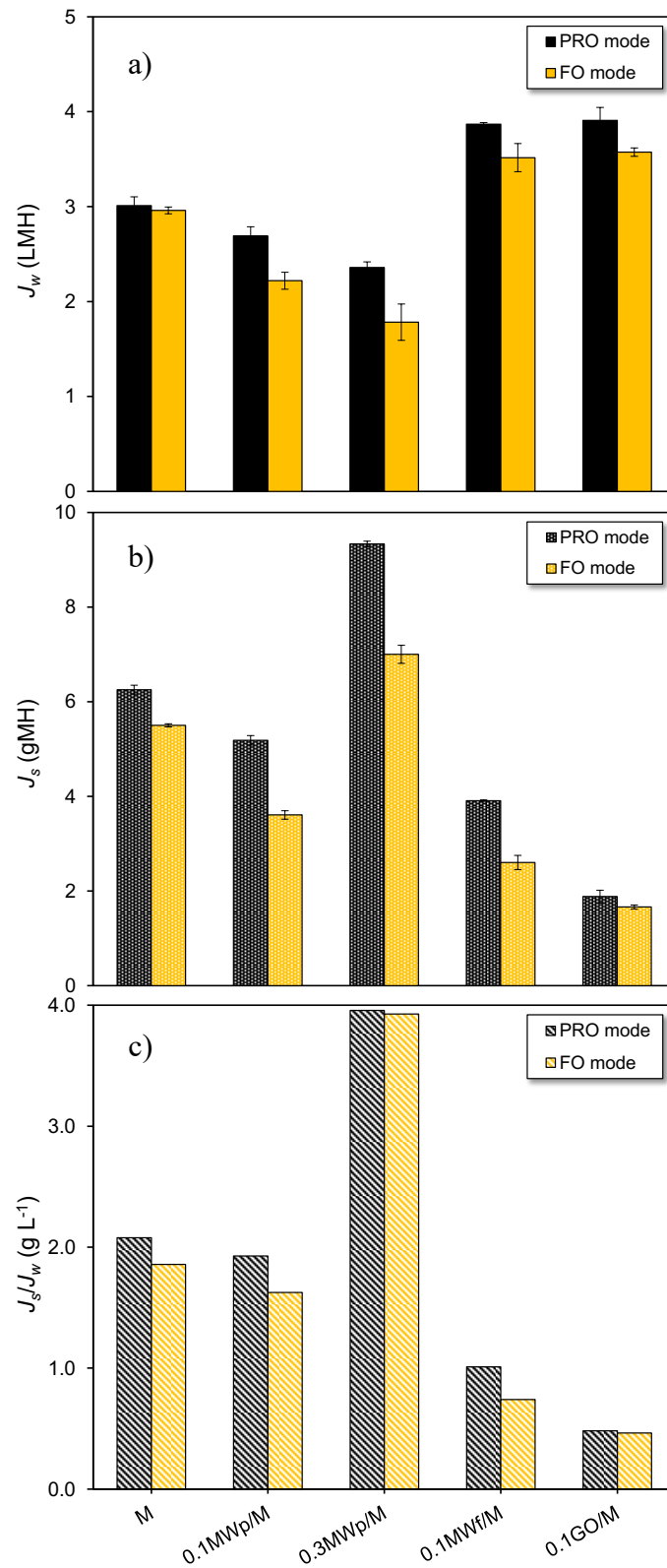


**Figure 5.** (a) Water flux ( $J_w$ ), (b) reverse solute flux ( $J_s$ ) and (c) specific solute flux ( $J_s/J_w$ ) obtained in both PRO and FO modes for TFC membranes prepared on different PSf supports.

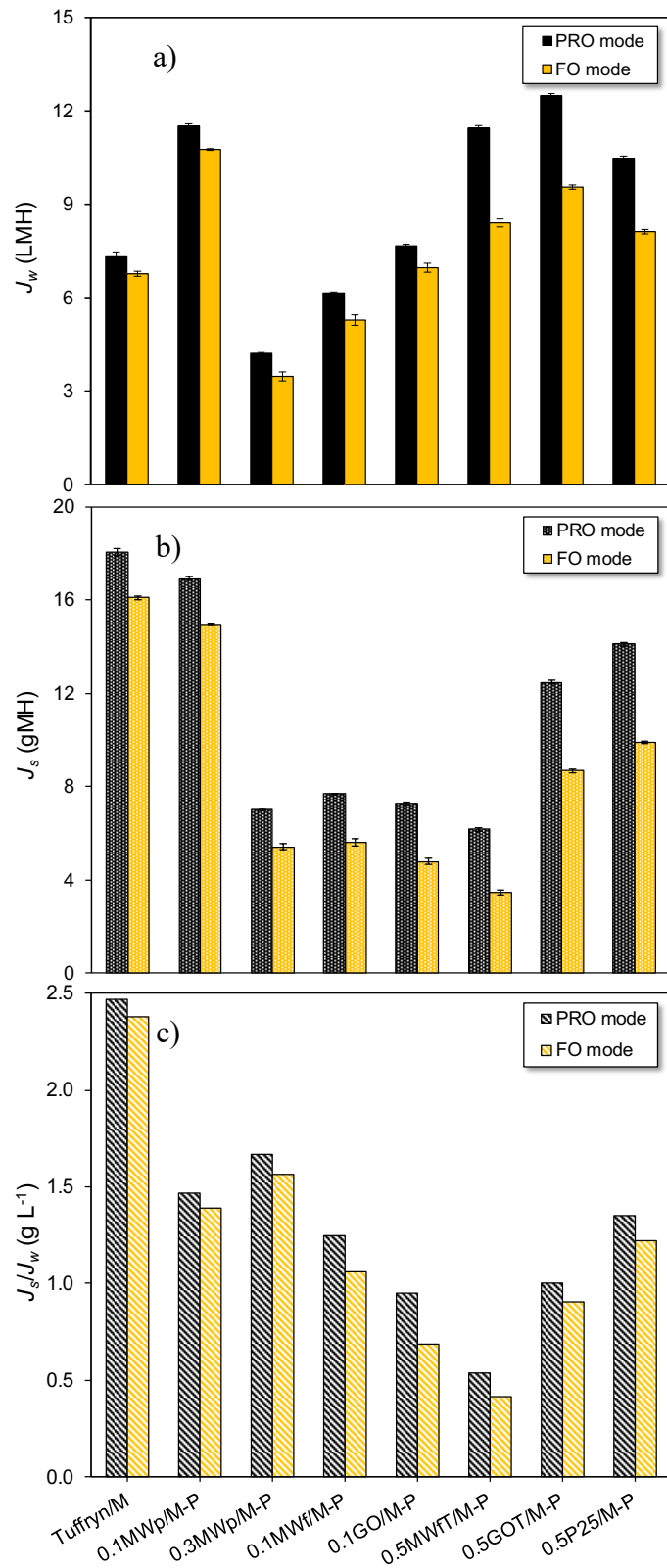


**Figure 6.** (a) Water flux ( $J_w$ ), (b) reverse solute flux ( $J_s$ ) and (c) specific solute flux ( $J_s/J_w$ ) obtained in both PRO and FO modes for TFC membranes prepared on different PSf-PVP supports.

### *3.4. Influence of the draw solution and membrane module configuration on the membrane performance in forward osmosis*

The draw solution properties and the membrane module are among the major factors influencing the FO performance. The most efficient 0.5MWfT/M-P membrane was studied in FO mode with different type and concentrations of draw solutions, as well as membrane module configurations. In this context, water flux, reverse solute flux and specific solute flux were analyzed using DI water (feed) and varying the NaCl solution concentration (Figure 7). An increase of the draw solution concentration usually leads to a higher osmotic pressure and, as consequence, to higher water fluxes. The results obtained for 0.5MWfT/M-P show a two-fold enhanced water flux with the higher NaCl concentration (e.g.,  $J_w \approx 8.4$  and  $17.1 \text{ L m}^{-2} \text{ h}^{-1}$  for 0.6 and 2.0 M NaCl, respectively). As observed, the increase of the water flux is not proportional to the draw solution concentration, due to an increase of the dilutive ICP with the draw solution concentration and, thereby, the overall gain of water is lower [49]. Furthermore, a higher NaCl concentration produced a considerable salt leakage (e.g.,  $J_s \approx 3.5$  and  $10.5 \text{ g m}^{-2} \text{ h}^{-1}$  for 0.6 and 2.0 M NaCl concentration, respectively), which increases the corresponding specific solute flux ( $J_s/J_w$ ).

The performance of 0.5MWfT/M-P was also investigated with three other draw solutions: KCl (monovalent ions), MgCl<sub>2</sub> (divalent cation and monovalent anion) and MgSO<sub>4</sub> (divalent ions). Among the selected draw solutions, MgCl<sub>2</sub> exhibits the highest osmotic pressure at 2.0 M concentration, both NaCl and KCl present similar intermediate osmotic pressures, and MgSO<sub>4</sub> has the lowest osmotic pressure. Thus, MgCl<sub>2</sub> is expected to generate the highest water flux; however, the measured water flux for 0.5MWfT/M-P decreased as follows: NaCl  $\leq$  KCl < MgCl<sub>2</sub> < MgSO<sub>4</sub>. This behaviour was previously reported for the case of CaCl<sub>2</sub> [49], and confirms that not only the osmotic pressure, but also the type of draw solution, plays a significant role in the FO performance [49].

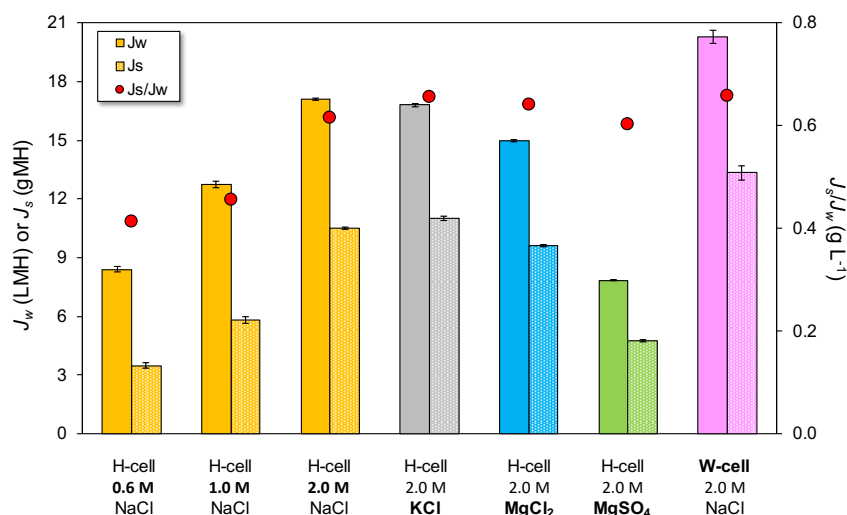


**Figure 7.** Water flux ( $J_w$ ), reverse solute flux ( $J_s$ ) and specific solute flux ( $J_s/J_w$ ) obtained in FO mode for 0.5MWfT/M-P by using different draw solutions and membrane modules.

The 0.5MWfT/M-P membrane was also tested in a specifically designed membrane module (W-cell, Figure S1) under the optimized draw solution conditions, a higher water permeation being observed in Figure 7 (i.e.,  $J_w \approx 17.1$  and  $20.3 \text{ L m}^{-2} \text{ h}^{-1}$  for H-cell and W-cell, respectively). This better performance obtained with the W-cell could be due to a decrease of the ICP, as consequence of the arrangement of the inlet streams. However, the specific solute flux was increased with the W-cell, although the value was quiet low ( $0.66 \text{ g L}^{-1}$ ). Table 3 compares the performance of the membranes prepared in this work with those reported in the literature at different feed and draw solutions.

**Table 3.** Comparison between the performance of the FO membrane prepared in this work and FO membranes reported in the literature.

Membrane	Feed solution	Draw solution	$J_w$ ( $\text{L m}^2 \text{ h}^{-1}$ )	$J_s$ ( $\text{g m}^2 \text{ h}^{-1}$ )	$J_s/J_w$ ( $\text{g L}^{-1}$ )	Ref.
0.5MWfT/M-P	DI water	1.0 M NaCl	12.7	5.8	0.46	This work
0.5MWfT/M-P	DI water	2.0 M NaCl	20.3	13.3	0.66	This work
0.05 wt.% pristine CNTs/PSf	DI water	2.0 M MgCl <sub>2</sub>	$\approx 9.2$	7.4	0.80	[26]
0.05wt.% functionalized CNTs/PEI	DI water	1.0 M NaCl	22.4	9.0	0.40	[50]

0.25 wt.% GO/PSf	DI water	0.5 M NaCl	19.8	3.4	0.17	[24]
0.5 wt. rGO modified graphitic carbon nitride/PES	DI water	2.0 M NaCl	41.4	≈ 9.5	0.23	[17]
2.0 wt. GO/PSf	DI water	1.0 M NaCl	9.2	3.8	0.41	[51]
2.0 wt. LDH/PSf	DI water	1.0 M NaCl	9.3	6.5	0.70	[51]
2.0 wt. LDH-GO/PSf	DI water	1.0 M NaCl	13.4	6.2	0.46	[51]
600 ppm GO/HPAN	DI water	2.0 M NaCl	≈ 32	≈ 7	0.22	[27]
0.6 wt.% TiO <sub>2</sub> /PSf	DI water	0.5 M NaCl	18.8	7.4	0.39	[9]
0.6 wt.% TiO <sub>2</sub> /PSf	DI water	2.0 M NaCl	33	15.7	0.48	[9]
TFC membrane (Oasys)	DI water	1.0 M NaCl	31.9	11.5	0.36	[52]
TFC membrane (HTI)	DI water	1.0 M NaCl	9.8	8.3	0.85	[52]
CTA membrane (HTI)	DI water	1.0 M NaCl	9.9	5.2	0.52	[52]

PEI: polyetherimide; PES: polyethersulfone; LDH: layered double hydroxide; HPAN: hydrolyzed polyacrylonitrile; HTI: Hydration Technology Innovations Company; CTA: Cellulose Triacetate.

#### 4. Conclusions

PSf supports blended with nanostructured materials, including pristine and functionalized MWCNTs, GO and carbon-TiO<sub>2</sub> composites, were prepared analysing different synthesis parameters. The surface hydrophilicity and the structure, in particular porosity, pore size and morphology of the PSf supports can be controlled by varying the loading, type and chemical properties of the material blended.

Hydrophobic MWCNTs (MW<sub>p</sub>) favour the formation of supports with macrovoids and high contact angles, while hydrophilic carbon materials (like MW<sub>f</sub> and GO) led to supports with lower contact angles, higher porosity and larger finger-like macrovoids when compared to the neat PSf support. The addition of a pore forming agent (PVP) and carbon-TiO<sub>2</sub> composites into PSf supports allowed to obtain a porous structure of more elongated and straight finger-like pores, and enhanced the surface hydrophilicity.

Selected PSf supports were used to prepare TFC membranes, whose performance was evaluated under PRO and FO modes, the following conclusions being highlighted:

- Hydrophilic carbon materials (i.e., GO and MW<sub>f</sub>) are preferred in TFC membranes, because they favour a higher water flux and a lower draw solute leakage, compared to membranes with

hydrophobic MWp or only neat PSf; this behaviour is explained by a more porous structure formed by larger finger-like macrovoids and a higher surface hydrophilicity induced by adding GO or MWf.

- The use of PVP in membranes containing hydrophobic MWp allows to achieve higher water fluxes than their analogues prepared with GO or MWf due to the formation of wider finger-like pores, although it also produced a lower selectivity towards NaCl.

- The addition of TiO<sub>2</sub>-based materials in TFC membranes containing PVP produced an enhanced permeation without sacrificing markedly the reverse solute flux. In particular, carbon-TiO<sub>2</sub> composites demonstrated to have a beneficial effect on TFC-membrane supports, a membrane prepared with 0.5 wt.% of a GO-TiO<sub>2</sub> composite and PVP being the most active in FO, in particular when compared with a TFC membrane prepared on a commercial PSf support (Tuffryn from Pall Corporation).

- Different types and concentrations of draw solutions, as well as the membrane module configuration may enhance the water permeation of TFC membranes in FO, although they also affect the salt leakage.

## **Acknowledgments**

Financial support for this work was provided by FCT and FEDER through COMPETE 2020 (Project UID/EQU/50020/2013 - POCI-01-0145-FEDER-006984) and by QREN, ON2, FCT and FEDER (NORTE-07-0124-FEDER-000015). SMT (SFRH/BPD/108981/2015) and AMTS (IF/01501/2013) acknowledge financial support from FCT, with financing from the European Social Fund and the Human Potential Operational Programme. Technical assistance by Dr. Carlos Sá and CEMUP team with SEM analysis is gratefully acknowledged. Dra. Hiléia K.S. Souza and Professor Maria P. Gonçalves are also acknowledged for kindly helping with the viscosity determinations.

## References

- [1] T.-S. Chung, S. Zhang, K.Y. Wang, J. Su, M.M. Ling, Forward osmosis processes: yesterday, today and tomorrow, *Desalination*, 287 (2012) 78-81.
- [2] D.L. Shaffer, J.R. Werber, H. Jaramillo, S. Lin, M. Elimelech, Forward osmosis: Where are we now?, *Desalination*, 356 (2015) 271-284.
- [3] X. Zhang, Z. Ning, D.K. Wang, J.C. Diniz da Costa, Processing municipal wastewaters by forward osmosis using CTA membrane, *Journal of Membrane Science*, 468 (2014) 269-275.
- [4] S. Zhao, L. Zou, C.Y. Tang, D. Mulcahy, Recent developments in forward osmosis: Opportunities and challenges, *Journal of Membrane Science*, 396 (2012) 1-21.
- [5] J.R. McCutcheon, M. Elimelech, Influence of membrane support layer hydrophobicity on water flux in osmotically driven membrane processes, *Journal of Membrane Science*, 318 (2008) 458-466.
- [6] H. Wu, B. Tang, P. Wu, Development of novel SiO<sub>2</sub>-GO nanohybrid/polysulfone membrane with enhanced performance, *Journal of Membrane Science*, 451 (2014) 94-102.
- [7] X. Liu, H.Y. Ng, Fabrication of layered silica-polysulfone mixed matrix substrate membrane for enhancing performance of thin-film composite forward osmosis membrane, *Journal of Membrane Science*, 481 (2015) 148-163.
- [8] D. Emadzadeh, W. Lau, A. Ismail, Synthesis of thin film nanocomposite forward osmosis membrane with enhancement in water flux without sacrificing salt rejection, *Desalination*, 330 (2013) 90-99.
- [9] D. Emadzadeh, W.J. Lau, T. Matsuura, A.F. Ismail, M. Rahbari-Sisakht, Synthesis and characterization of thin film nanocomposite forward osmosis membrane with hydrophilic nanocomposite support to reduce internal concentration polarization, *Journal of Membrane Science*, 449 (2014) 74-85.

- [10] N. Ma, J. Wei, R. Liao, C.Y. Tang, Zeolite-polyamide thin film nanocomposite membranes: Towards enhanced performance for forward osmosis, *Journal of Membrane Science*, 405–406 (2012) 149-157.
- [11] N. Ma, J. Wei, S. Qi, Y. Zhao, Y. Gao, C.Y. Tang, Nanocomposite substrates for controlling internal concentration polarization in forward osmosis membranes, *Journal of Membrane Science*, 441 (2013) 54-62.
- [12] M. Ghanbari, D. Emadzadeh, W.J. Lau, H. Riazi, D. Almasi, A.F. Ismail, Minimizing structural parameter of thin film composite forward osmosis membranes using polysulfone/halloysite nanotubes as membrane substrates, *Desalination*, 377 (2016) 152-162.
- [13] L. Dumée, J. Lee, K. Sears, B. Tardy, M. Duke, S. Gray, Fabrication of thin film composite poly(amide)-carbon-nanotube supported membranes for enhanced performance in osmotically driven desalination systems, *Journal of Membrane Science*, 427 (2013) 422-430.
- [14] J.H. Choi, J. Jegal, W.N. Kim, Fabrication and characterization of multi-walled carbon nanotubes/polymer blend membranes, *Journal of Membrane Science*, 284 (2006) 406-415.
- [15] A. Rahimpour, M. Jahanshahi, S. Khalili, A. Mollahosseini, A. Zirepour, B. Rajaeian, Novel functionalized carbon nanotubes for improving the surface properties and performance of polyethersulfone (PES) membrane, *Desalination*, 286 (2012) 99-107.
- [16] V. Vatanpour, S.S. Madaeni, R. Moradian, S. Zinadini, B. Astinchap, Fabrication and characterization of novel antifouling nanofiltration membrane prepared from oxidized multiwalled carbon nanotube/polyethersulfone nanocomposite, *Journal of Membrane Science*, 375 (2011) 284-294.
- [17] Y. Wang, R. Ou, H. Wang, T. Xu, Graphene oxide modified graphitic carbon nitride as a modifier for thin film composite forward osmosis membrane, *Journal of Membrane Science*, 475 (2015) 281-289.
- [18] J.K. Holt, Fast mass transport through sub-2-nanometer carbon nanotubes, *Science*, 312 (2006) 1034-1037.

- [19] K.S. Novoselov, A.K. Geim, S.V. Morozov, D. Jiang, Y. Zhang, S.V. Dubonos, I.V. Grigorieva, A.A. Firsov, Electric Field Effect in Atomically Thin Carbon Films, *Science*, 306 (2004) 666-669.
- [20] G. Romanos, L.M. Pastrana-Martínez, T. Tsoufis, C. Athanasekou, E. Galata, F. Katsaros, E. Favvas, K.G. Beltsios, E. Siranidi, P. Falaras, V. Psycharis, A.M.T. Silva, A facile approach for the development of fine-tuned self-standing graphene oxide membranes and their gas and vapor separation performance, *Journal of Membrane Science*, 493 (2015) 734-747.
- [21] L.M. Pastrana-Martínez, S. Morales-Torres, J.L. Figueiredo, J.L. Faria, A.M.T. Silva, Graphene oxide based ultrafiltration membranes for photocatalytic degradation of organic pollutants in salty water, *Water Research*, 77 (2015) 179-190.
- [22] S. Morales-Torres, T.L.S. Silva, L.M. Pastrana-Martinez, A.T.S.C. Brandao, J.L. Figueiredo, A.M.T. Silva, Modification of the surface chemistry of single- and multi-walled carbon nanotubes by HNO<sub>3</sub> and H<sub>2</sub>SO<sub>4</sub> hydrothermal oxidation for application in direct contact membrane distillation, *Physical Chemistry Chemical Physics*, 16 (2014) 12237-12250.
- [23] Y. Wang, R. Ou, Q. Ge, H. Wang, T. Xu, Preparation of polyethersulfone/carbon nanotube substrate for high-performance forward osmosis membrane, *Desalination*, 330 (2013) 70-78.
- [24] M.J. Park, S. Phuntsho, T. He, G.M. Nisola, L.D. Tijing, X.-M. Li, G. Chen, W.-J. Chung, H.K. Shon, Graphene oxide incorporated polysulfone substrate for the fabrication of flat-sheet thin-film composite forward osmosis membranes, *Journal of Membrane Science*, 493 (2015) 496-507.
- [25] M. Amini, M. Jahanshahi, A. Rahimpour, Synthesis of novel thin film nanocomposite (TFN) forward osmosis membranes using functionalized multi-walled carbon nanotubes, *Journal of Membrane Science*, 435 (2013) 233-241.
- [26] X. Song, L. Wang, C.Y. Tang, Z. Wang, C. Gao, Fabrication of carbon nanotubes incorporated double-skinned thin film nanocomposite membranes for enhanced separation performance and antifouling capability in forward osmosis process, *Desalination*, 369 (2015) 1-9.

- [27] L. Shen, S. Xiong, Y. Wang, Graphene oxide incorporated thin-film composite membranes for forward osmosis applications, *Chemical Engineering Science*, 143 (2016) 194-205.
- [28] L. He, L.F. Dumée, C. Feng, L. Velleman, R. Reis, F. She, W. Gao, L. Kong, Promoted water transport across graphene oxide–poly(amide) thin film composite membranes and their antibacterial activity, *Desalination*, 365 (2015) 126-135.
- [29] J. Yin, G. Zhu, B. Deng, Graphene oxide (GO) enhanced polyamide (PA) thin-film nanocomposite (TFN) membrane for water purification, *Desalination*, 379 (2016) 93-101.
- [30] H. Zhao, S. Qiu, L. Wu, L. Zhang, H. Chen, C. Gao, Improving the performance of polyamide reverse osmosis membrane by incorporation of modified multi-walled carbon nanotubes, *Journal of Membrane Science*, 450 (2014) 249-256.
- [31] M. Sianipar, S.H. Kim, C. Min, L.D. Tijing, H.K. Shon, Potential and performance of a polydopamine-coated multiwalled carbon nanotube/polysulfone nanocomposite membrane for ultrafiltration application, *Journal of Industrial and Engineering Chemistry*, 34 (2016) 364-373.
- [32] M. Safarpour, A. Khataee, V. Vatanpour, Thin film nanocomposite reverse osmosis membrane modified by reduced graphene oxide/TiO<sub>2</sub> with improved desalination performance, *Journal of Membrane Science*, 489 (2015) 43-54.
- [33] M. Kumar, Z. Gholamvand, A. Morrissey, K. Nolan, M. Ulbricht, J. Lawler, Preparation and characterization of low fouling novel hybrid ultrafiltration membranes based on the blends of GO–TiO<sub>2</sub> nanocomposite and polysulfone for humic acid removal, *Journal of Membrane Science*, 506 (2016) 38-49.
- [34] V. Vatanpour, S.S. Madaeni, R. Moradian, S. Zinadini, B. Astinchap, Novel antibifouling nanofiltration polyethersulfone membrane fabricated from embedding TiO<sub>2</sub> coated multiwalled carbon nanotubes, *Separation and Purification Technology*, 90 (2012) 69-82.
- [35] W.S. Hummers Jr, R.E. Offeman, Preparation of graphitic oxide, *Journal of the American Chemical Society*, 80 (1958) 1339-1339.

- [36] L.M. Pastrana-Martínez, S. Morales-Torres, V. Likodimos, J.L. Figueiredo, J.L. Faria, P. Falaras, A.M.T. Silva, Advanced nanostructured photocatalysts based on reduced graphene oxide-TiO<sub>2</sub> composites for degradation of diphenhydramine pharmaceutical and methyl orange dye, *Applied Catalysis B: Environmental*, 123-124 (2012) 241-256.
- [37] L.M. Pastrana-Martínez, S. Morales-Torres, S.K. Papageorgiou, F.K. Katsaros, G.E. Romanos, J.L. Figueiredo, J.L. Faria, P. Falaras, A.M.T. Silva, Photocatalytic behaviour of nanocarbon-TiO<sub>2</sub> composites and immobilization into hollow fibres, *Applied Catalysis B: Environmental*, 142-143 (2013) 101-111.
- [38] S. Brunauer, P.H. Emmett, E. Teller, Adsorption of gases in multimolecular layers, *Journal of the American Chemical Society*, 60 (1938) 309-319.
- [39] F. Rouquerol, J. Rouquerol, K. Sing, Adsorption by powders and porous solids: principles, methodology and applications, 1999, in, Academic Press, London.
- [40] T.L.S. Silva, S. Morales-Torres, J.L. Figueiredo, A.M.T. Silva, Multi-walled carbon nanotube/PVDF blended membranes with sponge- and finger-like pores for direct contact membrane distillation, *Desalination*, 357 (2015) 233-245.
- [41] J. Figueiredo, M. Pereira, M. Freitas, J. Orfao, Modification of the surface chemistry of activated carbons, *Carbon*, 37 (1999) 1379-1389.
- [42] S. Morales-Torres, L.M. Pastrana-Martínez, J.L. Figueiredo, J.L. Faria, A.M. Silva, Graphene oxide-P25 photocatalysts for degradation of diphenhydramine pharmaceutical and methyl orange dye, *Applied Surface Science*, 275 (2013) 361-368.
- [43] L.M. Pastrana-Martínez, S. Morales-Torres, V. Likodimos, P. Falaras, J.L. Figueiredo, J.L. Faria, A.M.T. Silva, Role of oxygen functionalities on the synthesis of photocatalytically active graphene-TiO<sub>2</sub> composites, *Applied Catalysis B: Environmental*, 158-159 (2014) 329-340.
- [44] D. Emadzadeh, W.J. Lau, T. Matsuura, M. Rahbari-Sisakht, A.F. Ismail, A novel thin film composite forward osmosis membrane prepared from PSf-TiO<sub>2</sub> nanocomposite substrate for water desalination, *Chemical Engineering Journal*, 237 (2014) 70-80.

- [45] M. Elimelech, W.A. Phillip, The Future of Seawater Desalination: Energy, Technology, and the Environment, *Science*, 333 (2011) 712-717.
- [46] M. Qasim, N.A. Darwish, S. Sarp, N. Hilal, Water desalination by forward (direct) osmosis phenomenon: A comprehensive review, *Desalination*, 374 (2015) 47-69.
- [47] P. Pardeshi, A.A. Mungray, Synthesis, characterization and application of novel high flux FO membrane by layer-by-layer self-assembled polyelectrolyte, *Journal of Membrane Science*, 453 (2014) 202-211.
- [48] Z. Wang, J. Tang, C. Zhu, Y. Dong, Q. Wang, Z. Wu, Chemical cleaning protocols for thin film composite (TFC) polyamide forward osmosis membranes used for municipal wastewater treatment, *Journal of Membrane Science*, 475 (2015) 184-192.
- [49] S. Phuntsho, S. Sahebi, T. Majeed, F. Lotfi, J.E. Kim, H.K. Shon, Assessing the major factors affecting the performances of forward osmosis and its implications on the desalination process, *Chemical Engineering Journal*, 231 (2013) 484-496.
- [50] M. Tian, Y.-N. Wang, R. Wang, Synthesis and characterization of novel high-performance thin film nanocomposite (TFN) FO membranes with nanofibrous substrate reinforced by functionalized carbon nanotubes, *Desalination*, 370 (2015) 79-86.
- [51] P. Lu, S. Liang, T. Zhou, X. Mei, Y. Zhang, C. Zhang, A. Umar, Q. Wang, Layered double hydroxide/graphene oxide hybrid incorporated polysulfone substrate for thin-film nanocomposite forward osmosis membranes, *RSC Advances*, 6 (2016) 56599-56609.
- [52] B.D. Coday, D.M. Heil, P. Xu, T.Y. Cath, Effects of Transmembrane Hydraulic Pressure on Performance of Forward Osmosis Membranes, *Environmental Science & Technology*, 47 (2013) 2386-2393.